Electronic Supplementary Material (ESI) for Journal of Materials Chemistry A.
This journal is © The Royal Society of Chemistry 2021

Supporting Information

Green Quasi-Solid-State Planar Asymmetric Supercapacitors with High Working Voltage and Extraordinary Volumetric Energy Density

Zhongyou Peng[a,b], Jun Huang[a,b], Qichang He[a,b], Shulong Li,[a,b] Licheng Tan[a,b], Yiwang Chen*[a,b,c,d]*

Z. Peng, J. Huang, Q. He, S. Li, Prof. Dr. L. Tan, Prof. Dr. Y. Chen

[a] College of Chemistry, Nanchang University, 999 Xuefu Avenue, Nanchang 330031, China.

[b] Institute of Polymers and Energy Chemistry (IPEC), Nanchang University, 999 Xuefu Avenue, Nanchang 330031, China.

[c] Institute of Advanced Scientific Research (iASR), Jiangxi Normal University, 99 Ziyang Avenue, Nanchang 330022, China.

[d] Key Laboratory of Functional Small Molecules for Ministry of Education, Jiangxi Normal University, 99 Ziyang Avenue, Nanchang 330022, China.

*Corresponding Authors: tanlicheng@ncu.edu.cn (L. Tan); ywchen@ncu.edu.cn (Y. Chen).

Experimental section

***Chemicals and materials*:** All the reagents and solvents, unless otherwise stated, were obtained from commercial sources (Sigma Aldrich, Alfa Aesar and Energy Chemical Inc. Shanghai.) and were used without further purification.

***Synthesis of $Na_{0.55}Mn_2O_4 \cdot 1.5H_2O$ nanosheets*:** $Na_{0.55}Mn_2O_4 \cdot 1.5H_2O$ nanosheets were synthesized by the molten salt method.[1] Typically, 10 g of sodium nitrate ($NaNO_3$) was added into a crucible and transferred to a muffle furnace with a preheat temperature of 350 °C. After $NaNO_3$ totally became molten, 0.4 g of manganese sulfate ($MnSO_4$) was added into the molten salt. After reacting at 350 °C for 2 min, the product was taken out of the furnace and cooled to the room temperature. Finally, the product was purified with ethanol and deionized water and dried at 80 °C overnight.

***Synthesis of 3D VN/rGO composite*:** Typically, 0.24 g commercial V_2O_5 and 60 mL of GO dispersed solution (2 mg mL^{-1}) were mixed homogeneously through magnetically stirring for 1 h. Then, the mixture was transferred to a 100 ml Teflon-lined autoclave and held at 180 °C for 12 h. The as-prepared sample was rinsed several times with deionized water and ethanol followed by freeze-drying for 2 days. Finally, the obtained product was heated at 600 °C for 3 h in a NH_3 (50 s.c.c.m.) atmosphere.

***Synthesis of pure VN nanobelts*:** 0.2 g commercial V_2O_5 and 0.2 g glucose were mixed into 60 mL deionized water and then magnetically stirred for 1 h. The mixture was transferred into a 100 mL Teflon-lined autoclave and held at 180 °C for 12 h. The as-prepared sample was washed several times with deionized water and ethanol followed

by freeze-drying for 2 days. Finally, the obtained product was heated at 600 °C for 3 h in a NH_3 (50 s.c.c.m.) atmosphere.

***Assembly of sandwich architecture ASCs*:** The cathode was prepared by spreading on carbon cloth a slurry containing the active material $Na_{0.55}Mn_2O_4 \cdot 1.5H_2O$, conductive carbon (Super P), and binder (PVDF) in a mass ratio of 7:2:1. The VN/rGO anode was fabricated using a similar method, with the mass ratio at 8:1:1. The gel electrolyte was prepared by adding 5 g of Na_2SO_4 and 3 g of carboxymethyl cellulose sodium (CMC) into 50 mL of deionized water under quick stirring at 90 °C for 3 h until the gel became transparent. Finally, the devices were sealed with PET films and Kapton tape.

Assembly of quasi-solid-state planar ASCs: the planar ASCs were fabricated by mask-assisted deposition method.[2,3] The EG nanosheets were prepared through electrochemical exfoliation of graphite in aqueous electrolyte.[4] The customized interdigital mask was composed of 8 interdigital fingers with 10 mm length, 1 mm width, and 1 mm width of interspace. As the optimized mass loading, 2 mL EG dispersion in ethanol solution (0.05 mg mL^{-1}) was firstly vacuum filtrated through a nylon membrane (0.22 μm) as current collectors with the help of the mask. Then, 1.0 mL mixed dispersion (0.5 mg mL^{-1}, 10 wt% EG) of $Na_{0.55}Mn_2O_4 \cdot 1.5H_2O$ and EG nanosheets, and 1 mL mixed dispersion (0.5 mg mL^{-1}, 10 wt% EG) of VN/rGO and EG nanosheets in ethanol solution were added onto the different sides of mask as cathode and anode, respectively. Subsequently, 2 mL EG dispersion (0.05 mg mL^{-1}) was filtered to form the second current collectors on the top of the active material layer. After peeling off the mask carefully, the interdigital electrodes on the membrane were transferred to a flexible PET or PI substrate. Finally, $Na_{0.55}Mn_2O_4$//VN/rGO planar

ASCs were obtained after drop casting CMC-Na_2SO_4 gel electrolyte on the project area of electrodes. Finally, the devices were sealed with PET films and Kapton tape. The packaging process is described as follows: First, the Cu conductive tape was pasted over the lead, the gel electrolyte was then coated on the electrodes. Second, the planar SC was placed between two thermoplastic films and sealed by thermoplastic sealing. Finally, the tip of the lead was fixed using an Kapton tape. For comparison, we also constructed $Na_{0.55}Mn_2O_4$//$Na_{0.55}Mn_2O_4$ planar SSCs, or VN/rGO//VN/rGO planar SSCs using the same mask-assisted deposition of the same volume of $Na_{0.55}Mn_2O_4 \cdot 1.5H_2O$ and EG, or VN/rGO and EG on two electrodes. Similarly, EG//EG planar SSCs were assembled only based on the EG electrodes.

***Assembly of self-powered systems*:** The self-powered systems were assembled by planar ASC device, commercial solar cell, and powered devices. First, the solar cell was used for harvesting and converting the solar energy into electric energy. Then, the planar ASC device was used in storing electric energy, and it can provide power to power devices.

***Materials characterizations*:** The field emission scanning electron microscopy (JEOL JSM-6700F, 15 keV), transmission electron microscopy (JEOL, JEM-2100F, 200 keV), and high-resolution transmission electron microscopy (HRTEM) were used to characterize the surface morphologies and microstructures of the samples. X-ray diffraction (XRD, PERSEE, XD-3 with Cu Kα radiation), energy-dispersive X-ray spectrometry (EDS, Tecnai G2 F30 S-TWIN), and X-ray photoelectron spectroscopy (XPS, Thermo-VG, ESCALAB 250) were used to examine the structure and phase purity of the samples. The crystalline structure was studied on a Bruker D8-A25

diffractometer with Cu Kα radiation (λ = 1.5406 Å). For phase identification and structure determination, the sample was loaded into 0.7 mm quartz capillaries, and synchrotron XRPD data were collected using a Mythen-II detector at powder diffraction beamline, Australian Synchrotron (ANSTO). The surface characteristics of the sample were studied by gas physisorption at 77 K on an automated apparatus (Micromeritics, ASAP 2010).

***Electrochemical measurements*:** All electrochemical measurements were evaluated with a CHI 660E electrochemical workstation (Chenhua, Shanghai). In the half-cell (three electrode), 1 M Na_2SO_4 was used as the electrolyte, and the as-prepared samples as the working electrode. A platinum plate counter electrode was used as the counter electrode and Ag/AgCl was used as the reference electrode. For the full cell (two electrode), CMC-Na_2SO_4 was used as electrolyte.

***Electrochemical calculations*:**

The specific capacitance C (F g^{-1}) of cathode and anode were calculated from the GCD or CV curves by using the following formula:

$$C_g = \frac{I\Delta t}{m\Delta V} \tag{1}$$

$$C = \frac{\int I(V)dV}{v * m\Delta V} \tag{2}$$

where I is the discharge current (A), Δt is the discharge time (s), m is the mass of the active material (g), ΔV is the voltage (V). v is scan rate (V s^{-1}).

In the two-electrode system, the electrochemical performance was calculated from the GCD or CV curves.

$$C_g = \frac{I\Delta t}{\Delta V} \tag{3}$$

$$C = \frac{\int I(V)dV}{v * \Delta V} \tag{4}$$

where C is the capacitance (F), I is the discharging current (A), Δt is the discharge time (s), v is the scan rate (V s^{-1}) and ΔV is the voltage (V).

For the device, the specific capacitance is calculated according the following equation:

$$C_m(S, V, M) = \frac{C}{m(S,V,M)} \tag{5}$$

where $C_m(S,V,M)$ is the areal, volumetric or mass specific capacitance (F cm^{-2}, F cm^{-3}, F g^{-1}), S is the area of devices (cm^{-2}), V is the volume of devices (cm^{-3}), m is the total mass of cathode and anode active material (g) and C is the capacitance (F).

The energy density E and power density P can be calculated according to the following equations:

$$E = \frac{C_m \Delta V^2}{2 \times 3.6} \tag{6}$$

where E_m is the energy density (Wh cm^{-2}, Wh cm^{-3} and Wh kg^{-1}), C_m is the specific capacitance, and ΔV is the voltage (V).

As for the power density, the calculated equation is

$$P = \frac{E}{\Delta t} \tag{7}$$

where P is the power density (W cm^{-2}, W cm^{-3} and W kg^{-1}), E is the energy density (Wh cm^{-2}, Wh cm^{-3} and Wh kg^{-1}), and Δt is the discharging time (h).

The contribution from diffusion-controlled process and surface reaction can be evaluated by using CV curves. The relationship between current *(I)* and scan rate *(v)* can be written as:

$$I = {}_a v^b \tag{8}$$

Where *a* and *b* are constant can be obtained from log *v* versus log *I* plots. Importantly, b-value gives valuable insight on charge storage kinetics. When b= 0.5 indicates an ideal diffusion-dominated process and when b = 1.0 indicates surface-determined capacitive-controlled behavior. Furthermore, the capacitive contribution to the total current can be differentiated quantitively by using the following equations:

$$I(V) = k_1 v + k_2 v^{\frac{1}{2}} \tag{9}$$

$$\frac{I(V)}{v^{\frac{1}{2}}} = k_1 v^{\frac{1}{2}} + k_2 \tag{10}$$

Where *I(V)* is the response current at a voltage (V), *v* is the scan rate (mV s^{-1}), k_1 and k_2 can be obtained from the slope and intercept, respectively. Where $k_1 v$ can be attributed to the current from surface capacitance contribution, while $k_2 v^{1/2}$ is indexed to the diffusion process.

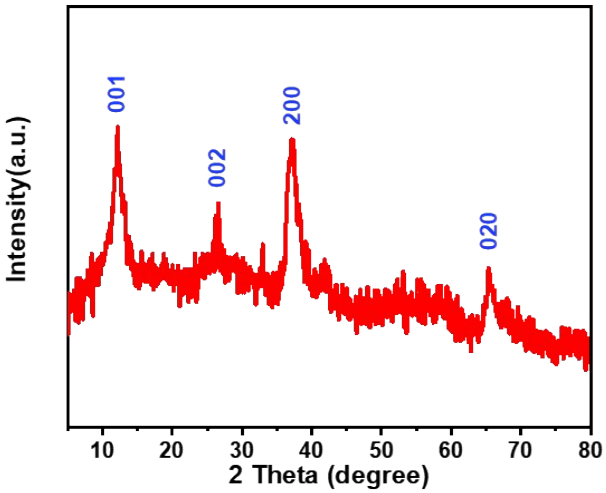

Fig. S1 XRD pattern of as-prepared $Na_{0.55}Mn_2O_4 \cdot 1.5H_2O$.

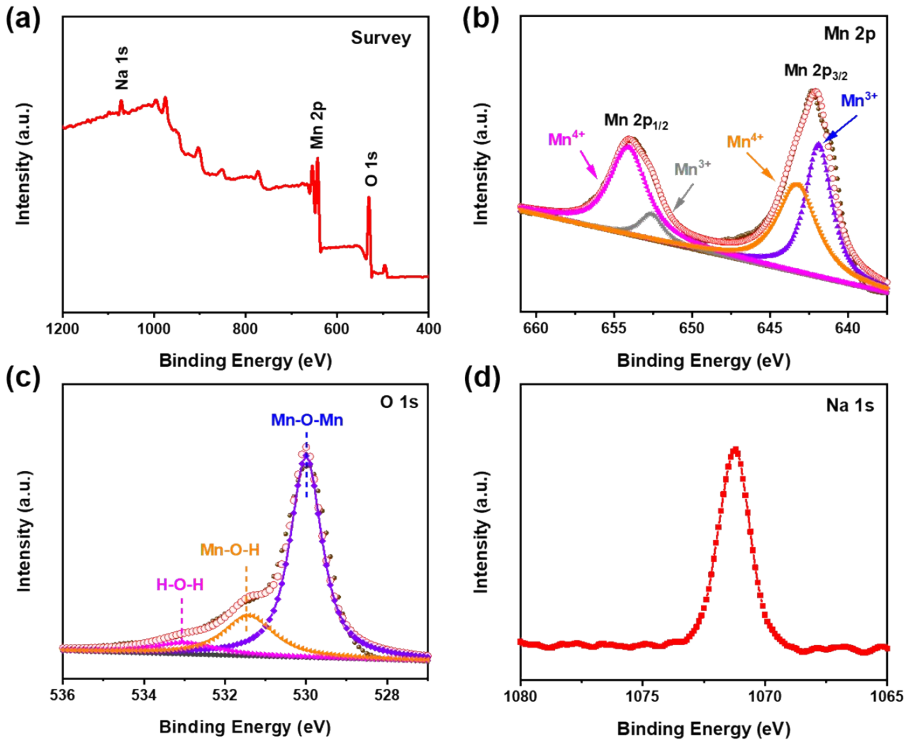

Fig. S2 XPS spectra of $Na_{0.55}Mn_2O_4 \cdot 1.5H_2O$: (a) survey, (b) Mn 2p, (c) O 1s, and (d) Na 1s.

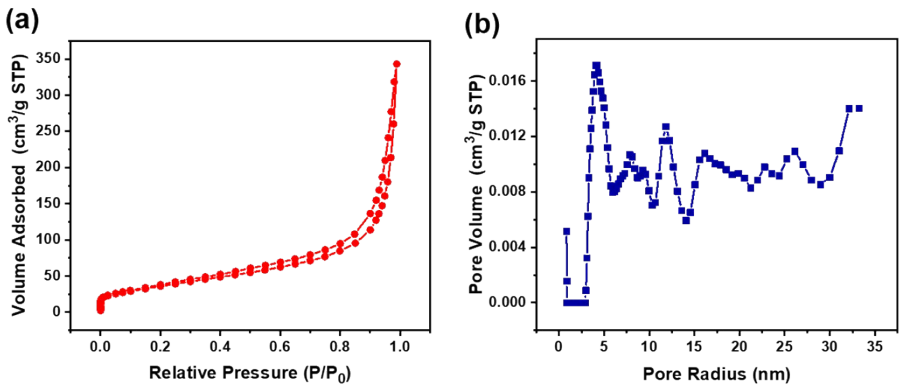

Fig. S3 (a) Nitrogen adsorption-desorption isotherms and (b) corresponding pore size distributions of $Na_{0.55}Mn_2O_4 \cdot 1.5H_2O$.

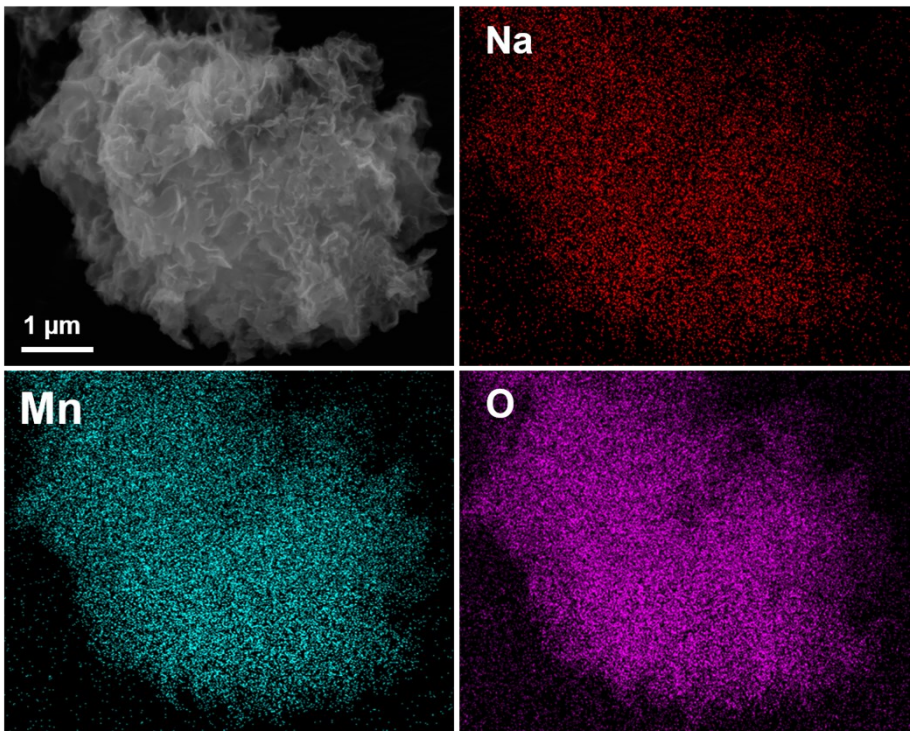

Fig. S4 SEM image and corresponding element mapping images of $Na_{0.55}Mn_2O_4 \cdot 1.5H_2O$ nanosheets.

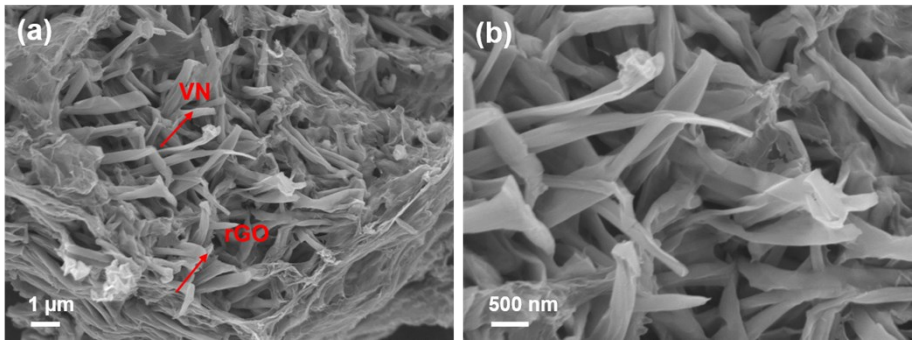

Fig. S5 SEM images of the prepared VN/rGO.

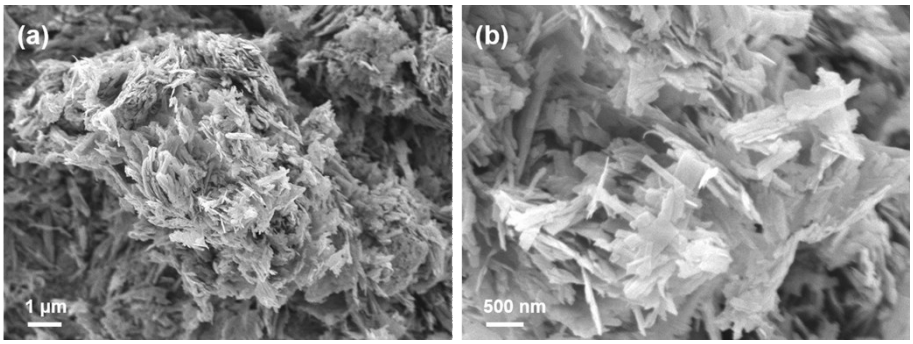

Fig. S6 SEM images of VN nanoribbons.

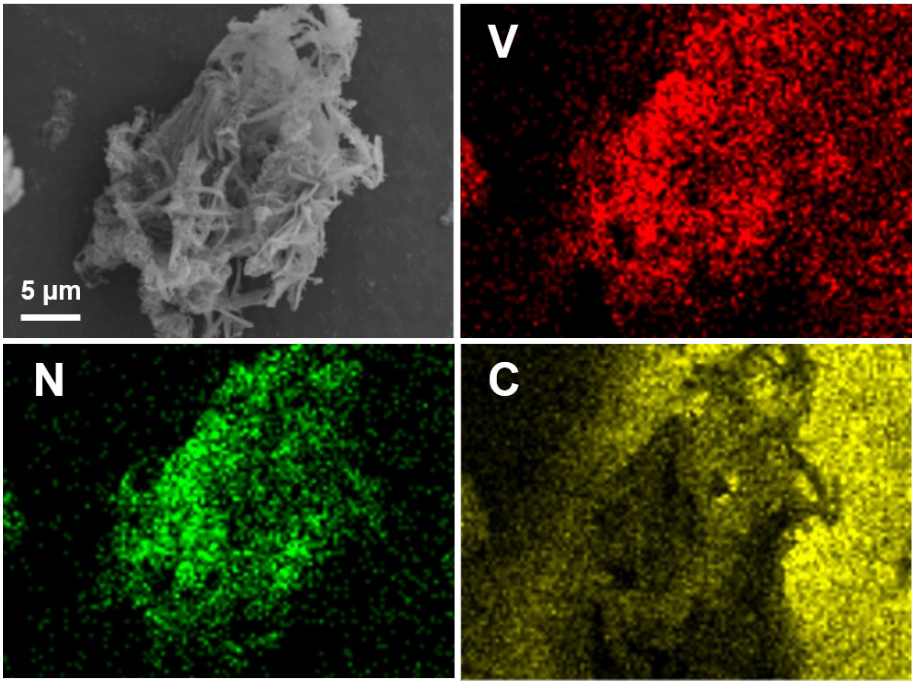

Fig. S7 SEM image and corresponding element mapping images of VN/rGO.

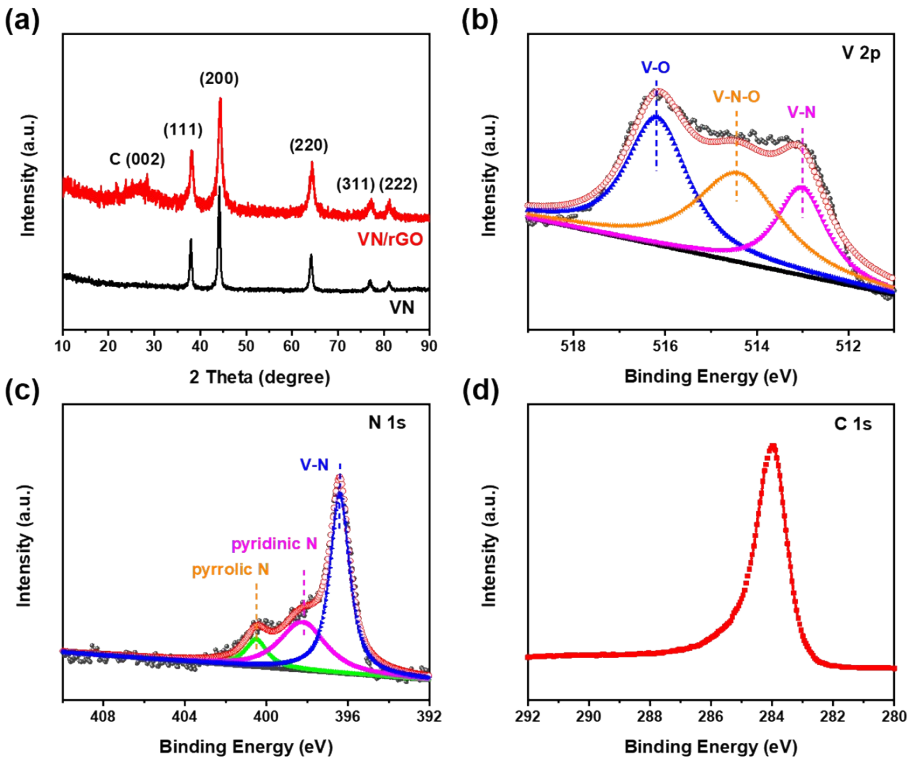

Fig. S8 (a) XRD patterns of the VN and VN/rGO. XPS spectra: (b) high-resolution V 2p, (c) N 1s and (d) C 1s of the VN/rGO.

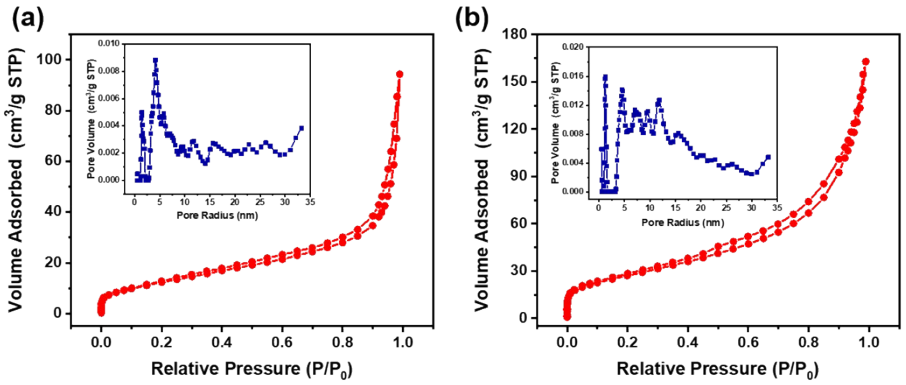

Fig. S9 N_2 adsorption/desorption isotherms of (a) pristine VN and (b) VN/rGO. The insets exhibit the pore size distribution of VN and VN/rGO, respectively.

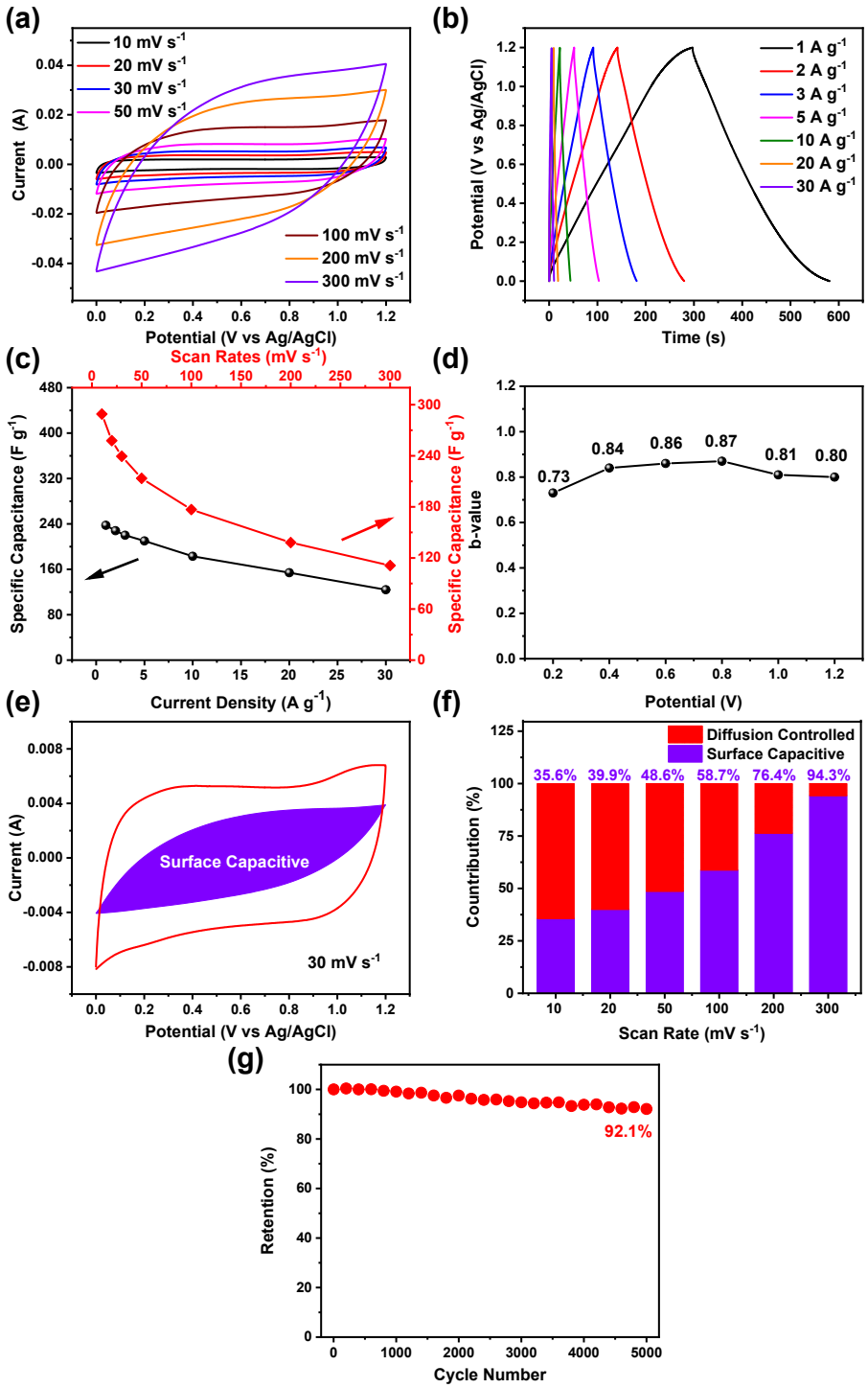

Fig. S10 (a) CV curves at different scan rates, (b) GCD curves at different current densities, (c) specific capacitance calculated from GCD and CV curves, (d) the b-values at various potentials, (e) capacitive and diffusion-controlled contributions to the total charge storage at 30 mV s^{-1}, (f) capacitance contribution differentiation, and (g) the cyclic stability of the $Na_{0.55}Mn_2O_4 \cdot 1.5H_2O$ electrode under a current density of 10 A g^{-1} after 5000 charge/discharge cycles.

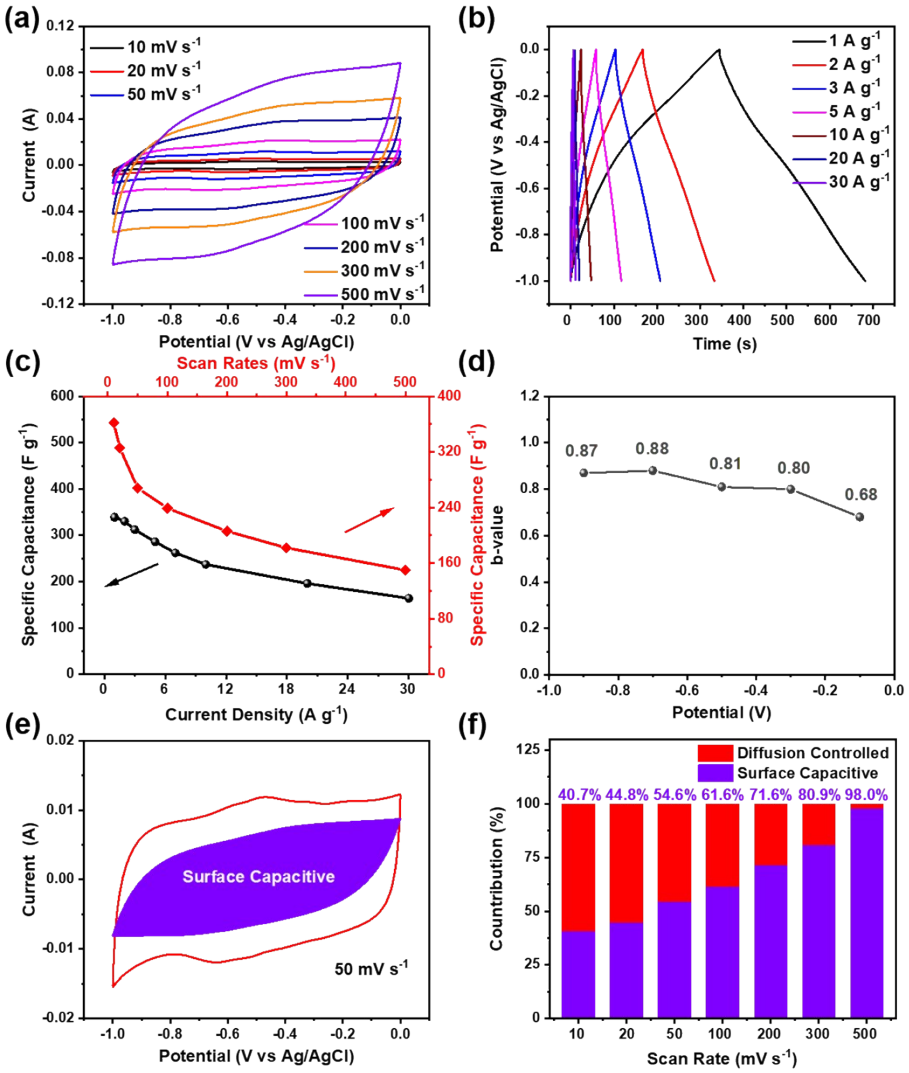

Fig. S11 (a) CV curves at different scan rates, (b) GCD curves at different current densities, (c) specific capacitance calculated from GCD and CV curves, (d) the b-values at various potentials, (e) capacitive and diffusion-controlled contributions to the total charge storage at 50 mV s^{-1} and (f) capacitance contribution differentiation of the VN/rGO electrode.

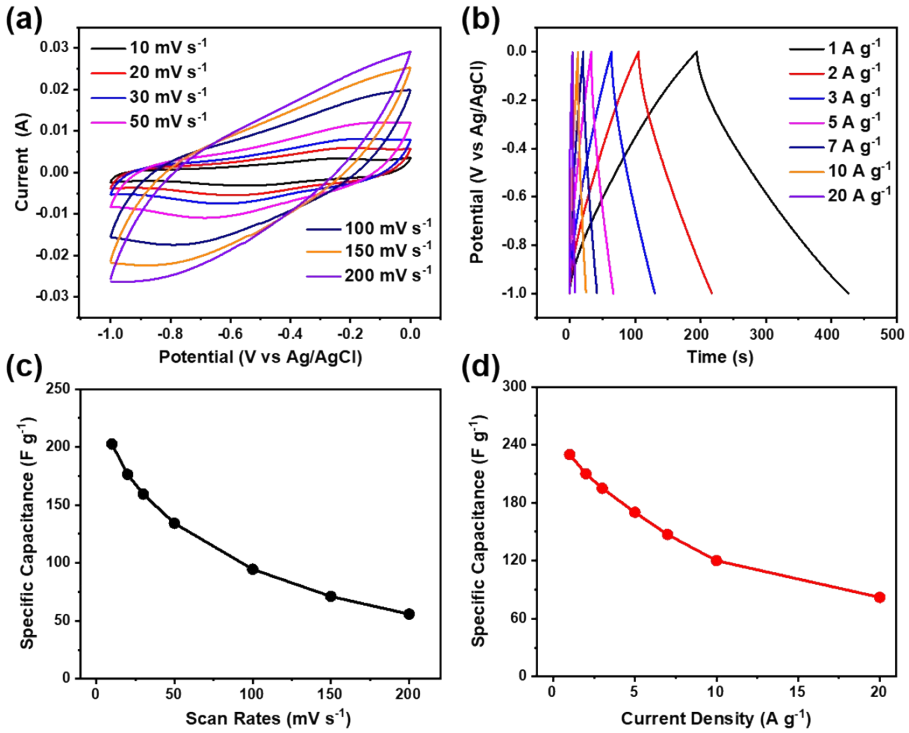

Fig. S12 (a) CV curves at different scan rates, (b) GCD curves at different current densities, specific capacitance calculated from (c) CV and (d) GCD curves of VN electrode.

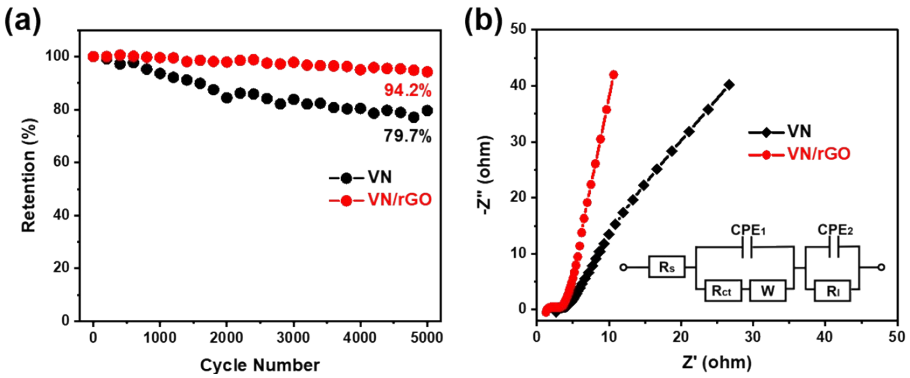

Fig. S13 (a) The cyclic stability under a current density of 10 A g^{-1} after 5000 charge/discharge cycles and (b) EIS spectra of VN and VN/rGO electrodes.

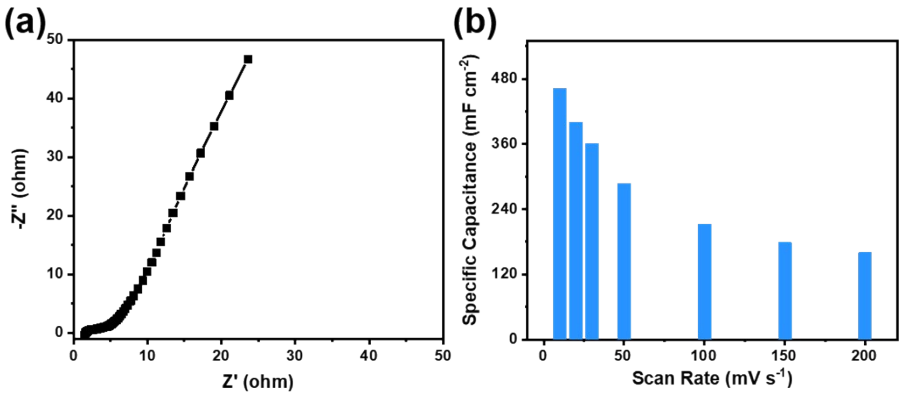

Fig. S14 (a) EIS spectrum and (b) areal specific capacitance at different current densities of the sandwich architecture ASC.

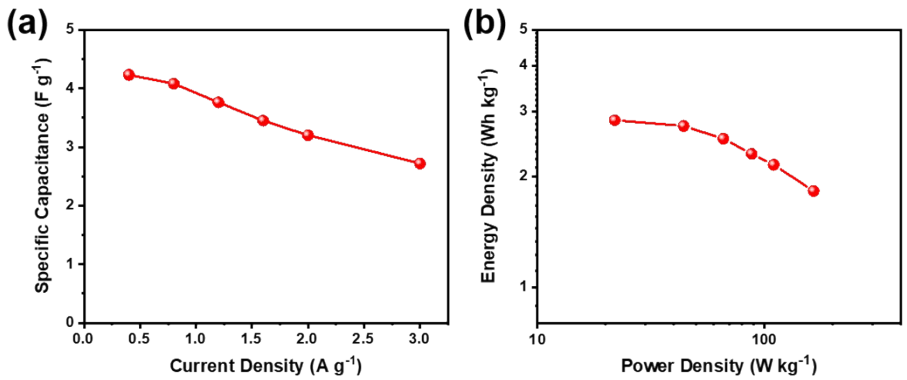

Fig. S15 (a) Specific capacitance and (b) Ragon plot of the quasi-solid-state sandwich ASC calculated from GCD curves based on the entire mass (including carbon cloth, active materials and electrolyte).

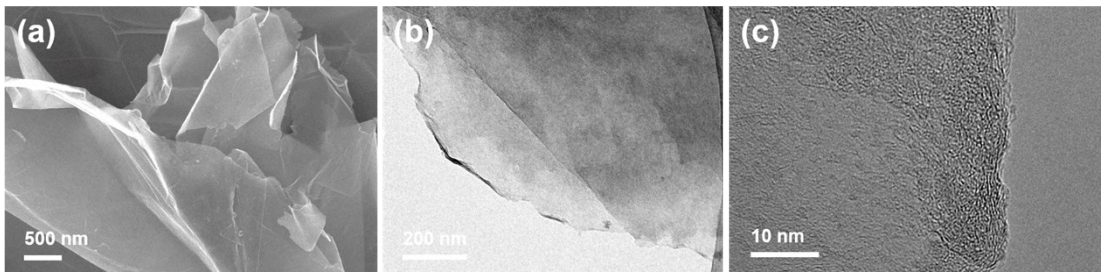

Fig. S16 (a) SEM, (b) TEM and (c) HRTEM images of EG nanosheets, revealing the uniform nanosheet morphology.

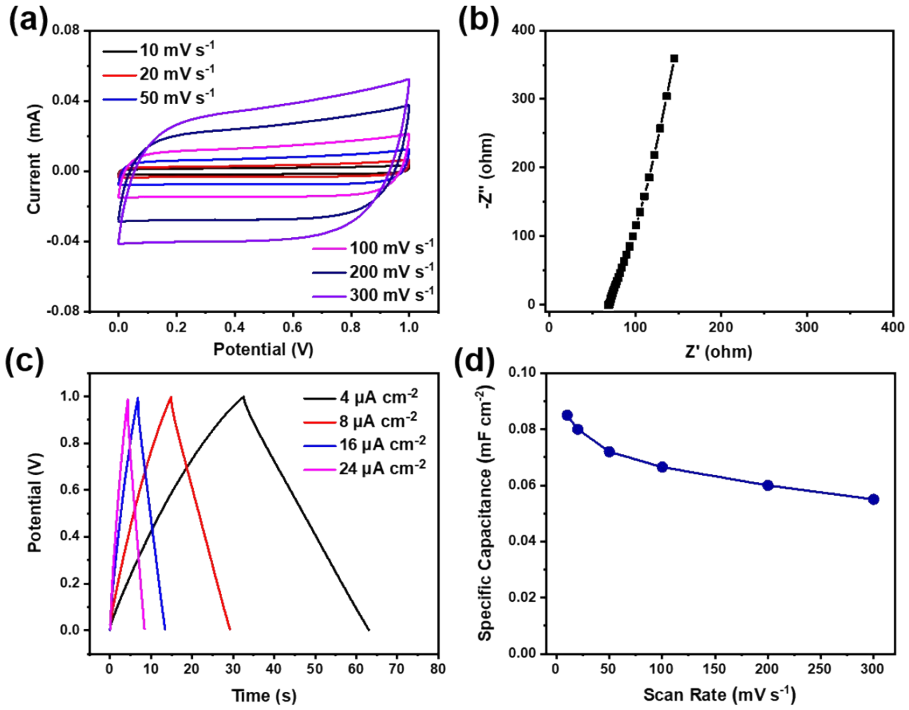

Fig. S17 (a) CV curves at different scan rates, (b) EIS spectrum, (c) GCD curves at various current densities, and (d) areal capacitance of EG//EG planar SSCs. It is calculated from the GCD curves that the areal capacitance is 0.09 mF cm^{-2}. Therefore, EG nanosheets in this work offered negligible capacitance contribution, and mainly served as metal-free current collectors.

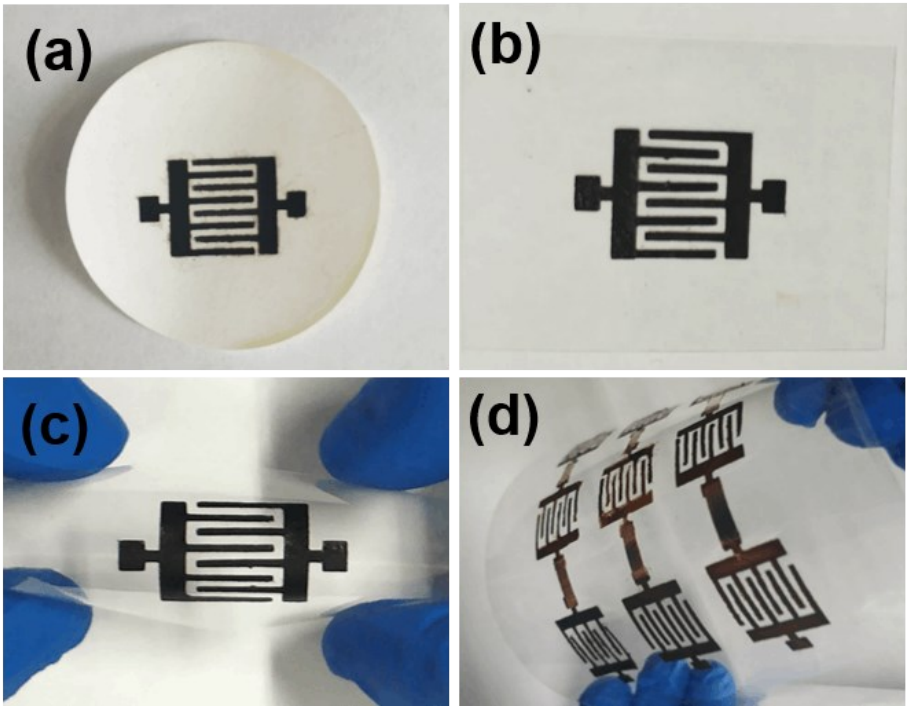

Fig. S18 (a) Photograph of the as-fabricated $Na_{0.55}Mn_2O_4$//VN/rGO interdigitated electrodes on the nylon membrane. (b,c) Transfer of interdigitated electrodes onto the PET substrate. (d) Photograph of nine $Na_{0.55}Mn_2O_4$//VN/rGO planar ASCs on a flexible PET substrate.

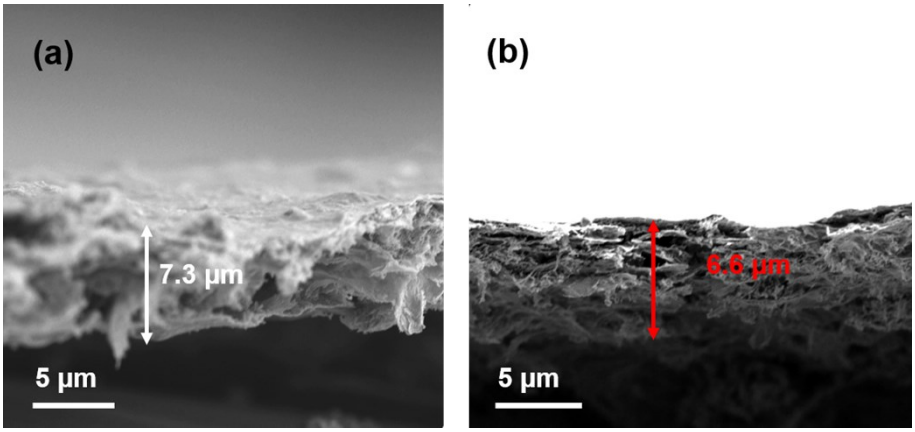

Fig. S19 Cross-section SEM images of (a) EG/$Na_{0.55}Mn_2O_4 \cdot 1.5H_2O$ cathode and (b) EG/VN/rGO anode.

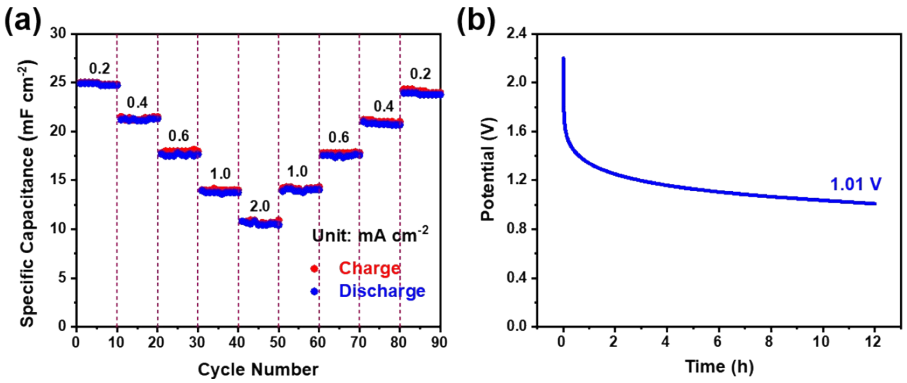

Fig. S20 (a) Cycling stability at different current densities, and (b) self-discharge measurement of the $Na_{0.55}Mn_2O_4$//VN/rGO planar ASC.

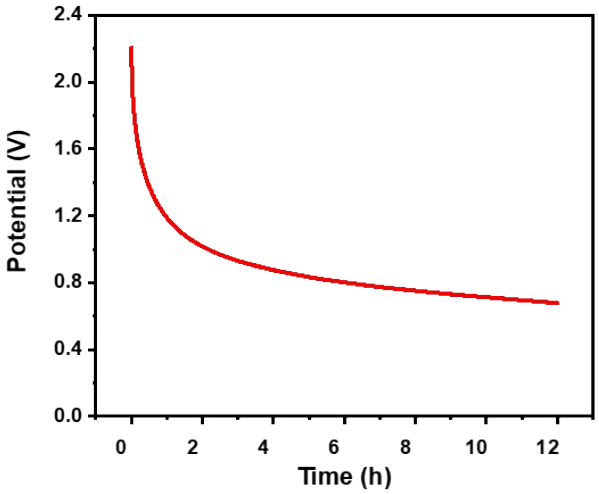

Fig. S21 self-discharge measurement of the solar-charging device.

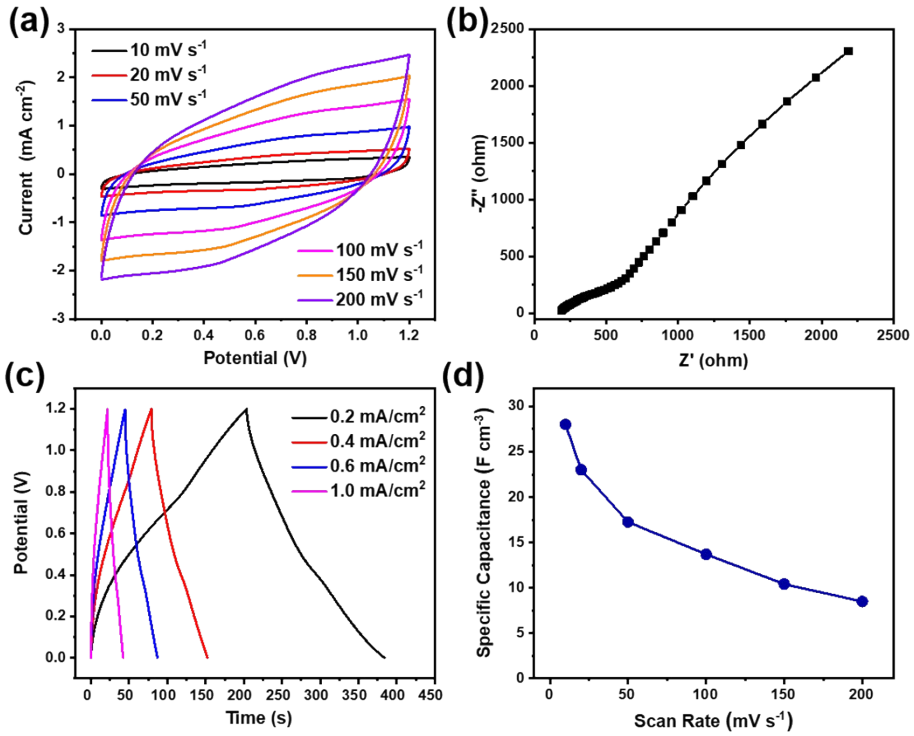

Fig. S22 (a) CV curves at different scan rates, (b) EIS spectrum, (c) GCD curves at various current densities, (d) volumetric capacitance of $Na_{0.55}Mn_2O_4$//$Na_{0.55}Mn_2O_4$ planar SSCs.

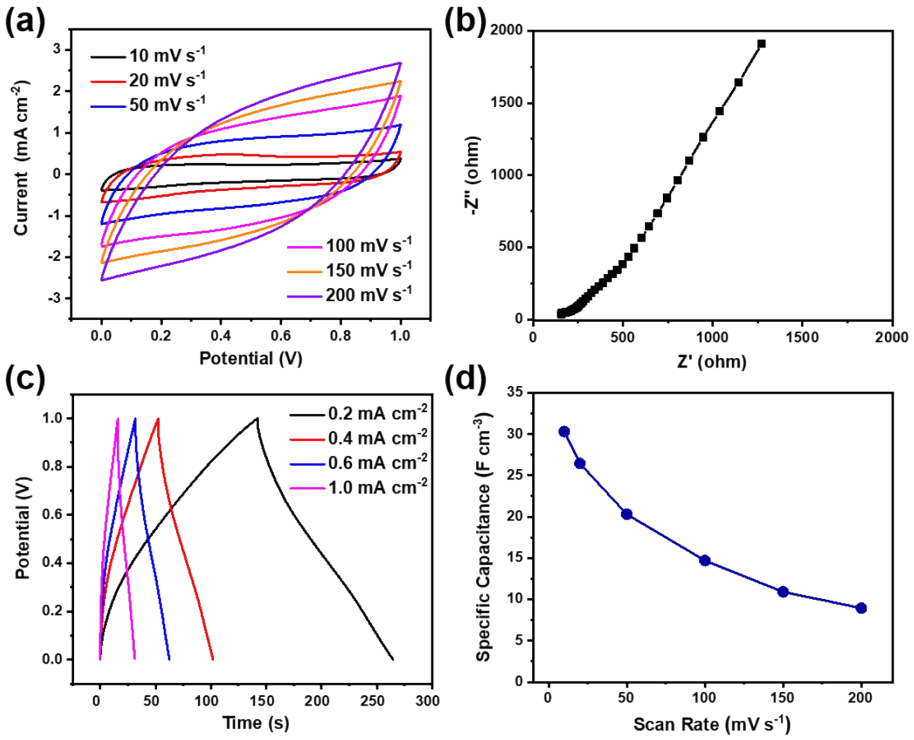

Fig. S23 (a) CV curves at different scan rates, (b) EIS spectrum, (c) GCD curves at various current densities, (d) volumetric capacitance of VN/rGO//VN/rGO planar SSCs.

Fig. S24 The thickness of the as-prepared flexible $Na_{0.55}Mn_2O_4$//VN/rGO planar ASCs based on the current collector, active material, gel electrolyte, and Kapton tape was measured by vernier caliper.

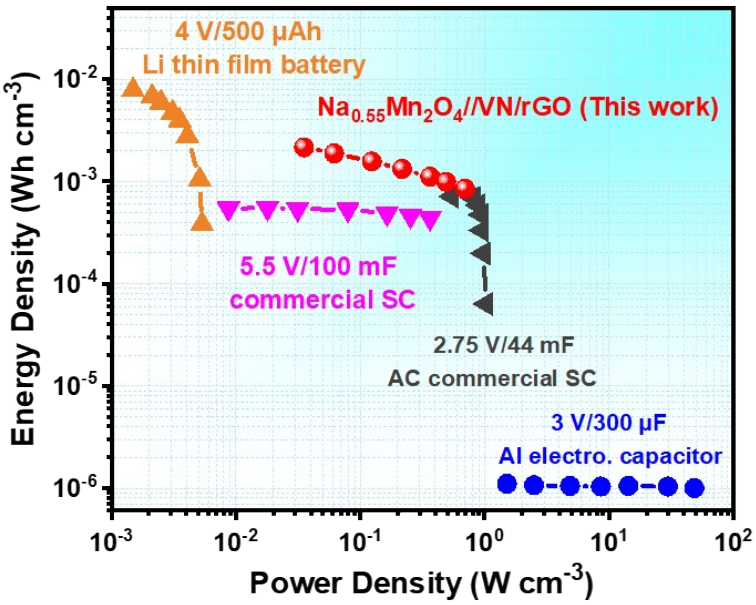

Fig. S25 Ragone plot comparing the energy and power densities of $Na_{0.55}Mn_2O_4$//VN/rGO planar ASCs based on the total volume of the full cell with commercially available energy storage devices.

Table S1. Refined structure parameters for $Na_{0.55}Mn_2O_4 \cdot 1.5H_2O$ listing fractional coordinates (x, y, z) and occupancies (Occ.).

Atom	x	y	z	Occ.
Na1	0.0000	0.0000	0.3754	1
Mn1	0.3489	0.1662	0.0000	1
O1	0.1545	0.2030	0.0000	1
O2	0.5421	0.1650	0.0000	1

Table S2. Electrochemical properties for $Na_{0.55}Mn_2O_4 \cdot 1.5H_2O$ electrode in comparison with those Mn-based electrode materials in earlier reports. *V*: voltage window (V vs. Ag/AgCl or SCE); *C*: specific capacitance (F g^{-1}); *R*: rate capability (F g^{-1}).

Mn-based electrodes	Electrolyte	*V*	*C*	*R*	Ref.
m-MnO_2 nanosheets	5 M LiTFSI	0 to 1.0 V	243 at 1 mV s^{-1}	--	2
MnO_2/GO	1 M Na_2SO_4	-0.1 to 0.9 V	297 at 5 mV s^{-1}	268 at 50 mV s^{-1}	5
MnO_2@PPy NWs	1 M Na_2SO_4	0 to 0.9 V	325 at 1 A g^{-1}	170 at 30 A g^{-1}	6
rGO@Mn_3O_4	1 M Na_2SO_4	-0.1 to 1.2 V	288 at 0.7 A g^{-1}	174 at 24 A g^{-1}	7
3D Mn_3O_4	1 M Na_2SO_4	0 to 1.0 V	274 at 0.5 A g^{-1}	52.7 at 30 A g^{-1}	8
HCC@MnO_2	1 M LiCl	0 to 0.8 V	243 at 1 A g^{-1}	139 at 10 A g^{-1}	9
D-MnO_2	1 M Na_2SO_4	0 to 0.8 V	202 at 1 A g^{-1}	137 at 20 A g^{-1}	10
rGO/MnO_x	0.5 M Na_2SO_4	0 to 0.8 V	202 at 1 mV s^{-1}	--	11
α-MnO_2	1 M Na_2SO_4	0 to 0.9 V	304 at 3 mA cm^{-2}	--	12
α-MnO_2@δ-MnO_2	1 M Na_2SO_4	0 to 1.0 V	206 at 0.25 A g^{-1}	170.1 at 2 A g^{-1}	13
$Na_{0.55}Mn_2O_4 \cdot 1.5H_2O$	**1 M Na_2SO_4**	**0 to 1.2 V**	**289 at 10 mV s^{-1}** **238 at 1 A g^{-1}**	**111 at 300 mV s^{-1}** **124 at 30 A g^{-1}**	**This work**

Table S3. Electrochemical properties of VN/rGO electrode in comparison with other anode materials in earlier reports. *V*: voltage window (V vs. Ag/AgCl or SCE); *C*: specific capacitance (F g^{-1}); *R*: rate capability (F g^{-1}).

Electrode materials	Electrolyte	*V*	*C*	*R*	Ref.
VN nanosheets	5 M LiTFSI	-1 to 0 V	121 at 1 mV s^{-1}	--	2
rGO@VO_2	1 M Na_2SO_4	-1 to 0 V	326 at 0.85 A g^{-1}	118 at 17 A g^{-1}	7
Graphene/MoO_3	1 M Na_2SO_4	-1 to 0 V	291 at 2 mV s^{-1}	--	14
VN	1 M $MgSO_4$	-0.9 to 0 V	230 at 10 mV s^{-1}	--	15
VN/PEDOT	1 M KOH	-1.2 to -0.2 V	226.2 at 1 A g^{-1}	175.9 at 1 A g^{-1}	16
MoO_3@CNT	1 M Na_2SO_4	-1 to 0 V	281 at 1 mV s^{-1}	79 at 200 mV s^{-1}	17
γ-Fe_2O_3/graphene	1 M Na_2SO_3	-0.8 to 0 V	224 at 1 A g^{-1}	203.8 at 20 A g^{-1}	18
VN	6 M KOH	-1.2 to 0 V	231 at 20 mV s^{-1}	122 at 100 mV s^{-1}	19
Fe_2O_3 nanotube	5 M LiCl	-0.8 to 0 V	257.8 at 1.4 A g^{-1}	--	20
VN/rGO	**1 M Na_2SO_4**	**-1 to 0 V**	**362 at 10 mV s^{-1}** **339 at 1 A g^{-1}**	**182 at 300 mV s^{-1}** **164 at 30 A g^{-1}**	**This work**

Table S4. Comparison study on the electrochemical performance of sandwich architecture ASC in this work with previously reported results. *V*: voltage window (V); *E*: maximum energy density (mWh cm^{-3}); *P*: maximum power density (W cm^{-3}).

Active materials	Electrolyte	*V*	*E*	*P*	Ref.
MnO_2//Fe_2O_3	PVA/LiCl	1.6	0.55	0.14	20
V_2O_3@C//Fe_3O_4@TiO_2	PVA/LiCl	2.0	2.23	1.09	21
MnO_2/ZnO//RGO	PVA/LiCl	1.8	0.234	0.133	22
α-Fe_2O_3@PANI//PANI	Na_2SO_4	1.5	0.315	0.3	23
MnO_2//RGO	PVA/LiCl	1.8	0.25	1.44	24
H-TiO_2@MnO_2//H-TiO_2@C	PVA/LiCl	1.8	0.3	0.23	25
MnO_2//Ti-Fe_2O_3@PEDOT	PVA/LiCl	1.6	0.89	0.44	26
VN//VO_X	PVA/LiCl	1.8	0.61	0.85	27
ASV-FO//V-CO	PVA/LiCl	1.6	0.95	--	28
VO_x@MoO_3//MnO_2	LiCl	2.0	3.02	0.65	29
Ni/MnO_2//Ni/AC	LiCl	2.5	0.78	0.05	30
CNT/MnO_2//CNT/PPy	PAAM/LiCl	2.0	0.31	0.06	31
CNTs//Fe_3O_4-C	PVA/KOH	1.7	1.56	0.48	32
$Na_{0.55}Mn_2O_4$//VN/rGO	**CMC/Na_2SO_4**	**2.2**	**3.89**	**0.41**	**This work**

Table S5. Comparison study on the electrochemical performance of planar SCs in this work with previously reported results. V: voltage window (V); C_v: volumetric capacitance (F cm^{-3}); E_v: maximum volumetric energy density (mWh cm^{-3}); P_v: maximum volumetric power density (W cm^{-3}).

Electrode materials	Electrolyte	V	C_v	E_v	P_v	Ref.
VN//MnO_2	SiO_2/LiTFSI	2.0	38.8	21.6	1.54	2
PPy/graphene	PVA/H_2SO_4	0.8	110	2.5	0.397	33
N-doped graphene	PVA/H_3PO_4	0.8	3.4	0.3	0.2	34
graphene/CNT carpets	Na_2SO_4	1.0	1.08	2.42	115	35
MWNT/Mn_3O_4	PMMA/PC/$LiClO_4$	1.2	8.9	1.8	0.06	36
LIG-FeOOH//LIG-MnO_2	PVA/LiCl	1.8	5.4	2.4	2.89	37
V_2O_5-PANI//MnO_2-PPy	PVA/LiCl	1.6	--	19.8	2.57	38
LSG/RuO_2//AC	Na_2SO_4	1.8	8.6	5	5	39
Fe_2O_3//MnO_2	KOH	1.2	60	12	14.8	40
$Na_{0.55}Mn_2O_4$//$Na_{0.55}Mn_2O_4$	**CMC/Na_2SO_4**	**1.2**	**28.0**	**5.6**	**1.0**	**This work**
VN/rGO/VN/rGO	**CMC/Na_2SO_4**	**1.0**	**30.3**	**4.2**	**0.9**	**This work**
$Na_{0.55}Mn_2O_4$//VN/rGO	**CMC/Na_2SO_4**	**2.2**	**40.5**	**27.3**	**8.8**	**This work**

References

1 Z. Hu, X. Xiao, H. Jin, T. Li, M. Chen, Z. Liang, Z. Guo, J. Li, J. Wan, L. Huang, Y. Zhang, G. Feng and J. Zhou, *Nat. Commun*., **2017**, *8*, 15630.

2 J. Qin, S. Wang, F. Zhou, P. Das, S. Zheng, C. Sun, X. Bao and Z.-S. Wu, *Energy Storage Mater*., **2019**, *18*, 397-404.

3 F. Zhou, H. Huang, C. Xiao, S. Zheng, X. Shi, J. Qin, Q. Fu, X. Bao, X. Feng, K. Müllen and Z.-S. Wu, *J. Am. Chem. Soc*., **2018**, *140*, 8198-8205.

4 K. Parvez, Z.-S. Wu, R. Li, X. Liu, R. Graf, X. Feng and K. Müllen, *J. Am. Chem. Soc*., **2014**, *136*, 6083-6091.

5 Y. Zhao, W. Ran, J. He, Y. Huang, Z. Liu, W. Liu, Y. Tang, L. Zhang, D. Gao and F. Gao, *Small,* **2015**, *11*, 1310-1319.

6 W. He, C. Wang, F. Zhuge, X. Deng, X. Xu and T. Zhai, *Nano Energy,* **2017**, *35*, 242-250.

7 R. Sahoo, D. T. Pham, T. H. Lee, T. H. T. Luu, J. Seok and Y. H. Lee, *ACS Nano,* **2018**, *12*, 8494-8505.

8 S. Li, L.-L. Yu, R.-B. Li, J. Fan and J.-T. Zhao, *Energy Storage Mater.,* **2018**, *11*, 176-183.

9 Z. Chen, L. Zheng, T. Zhu, Z. Ma, Y. Yang, C. Wei, L. Liu and X. Gong, *Adv. Electron. Mater.,* **2019**, *5*, 180072.

10 Y.-P. Zhu, C. Xia, Y. Lei, N. Singh, U. Schwingenschlögl and H. N. Alshareef, *Nano Energy,* **2019**, *56*, 357-364.

11 Y. Wang, W. Lai, N. Wang, Z. Jiang, X. Wang, P. Zou, Z. Lin, H. J. Fan, F. Kang, C.-P. Wong and C. Yang, *Energy Environ. Sci.,* **2017**, *10*, 941-949.

12 Z. H. Huang, Y. Song, D. Y. Feng, Z. Sun, X. Sun and X. X. Liu, *ACS Nano,* **2018**, *12*, 3557-3567.

13 Y. Guo, L. Li, L. Song, M, Wu, Y. Gao, J. Chen, C. Mao, J. Song and H. Niu, *J. Mater. Chem. A*, **2019**, *7*. 12661-12668.

14 J. Chang, M. Jin, F. Yao, T. H. Kim, V. T. Le, H. Yue, F. Gunes, B. Li, A. Ghosh, S. Xie and Y. H. Lee, *Adv. Funct. Mater*., **2013**, *23*, 5074-5083.

15 Z. Tian, X. Tong, G. Sheng, Y. Shao, L. Yu, V. Tung, J. Sun, R. B. Kaner and Z. Liu, *Nat. Commun*., **2019**, *10*, 4913.

16 M. Chen, H. Fan, Y. Zhang, X. Liang, Q. Chen and X. Xia, *Small,* **2020**, *16*, 2003434.

17 T. H. Lee, D. T. Pham, R. Sahoo, J. Seok, T. H. T. Luu and Y. H. Lee, Energy Storage Mater., **2018**, *12*, 223-231.

18 H.-C. Chen, C.-C. Wang and S.-Y. Lu, *J. Mater. Chem. A,* **2014**, 2, 16955-16962.

19 Y. Yi, L. Yu, Z. Tian, Y. Song, Y. Shao, L. Gao, J. Sun and Z. Liu, *Adv. Funct. Mater.,* **2018***, 28,* 1805510.

20 P. Yang, Y. Ding, Z. Lin, Z. Chen, Y. Li, P. Qiang, M. Ebrahimi, W. Mai, C. P. Wong and Z. L. Wang, *Nano Lett*., **2014**, *14*, 731-736.

21 R. Li, X. Ba, H. Zhang, P. Xu, Y. Li, C. Cheng and J. Liu, *Adv. Funct. Mater.,* **2015***, 25,* 5384.

22 W. Zilong, Z. Zhu, J. Qiu and S. Yang, *J. Mater. Chem. C,* **2014**, *2*, 1331-1336.

23 X. F. Lu, X. Y. Chen, W. Zhou, Y. X. Tong and G. R. Li, *ACS Appl. Mater. Interfaces,* **2015**, *7*, 14843-14850.

24 T. Zhai, S. Xie, M. Yu, P. Fang, C. Liang, X. Lu and Y. Tong, *Nano Energy,* **2014**, *8*, 255-263.

25 X. Lu, M. Yu, G. Wang, T. Zhai, S. Xie, Y. Ling, Y. Tong and Y. Li, *Adv. Mater.,* **2013**, *25*, 267-272.

26 Y. Zeng, Y. Han, Y. Zhao, Y. Zeng, M. Yu, Y. Liu, H. Tang, Y. Tong and X. Lu,

Adv. Energy Mater., **2015***, 5,* 1402176.

27 X. Lu, M. Yu, T. Zhai, G. Wang, S. Xie, T. Liu, C. Liang, Y. Tong and Y. Li, *Nano Lett.,* **2013**, *13*, 2628-2633.

28 S. Sun, T. Zhai, C. Liang, S. V. Savilov and H. Xia, *Nano Energy,* **2018**, *45*, 390-397.

29 S.-Q. Wang, X. Cai, Y. Song, X. Sun and X.-X. Liu, *Adv. Funct. Mater.,* **2018***, 28,* 1800497.

30 L. Zhang, P. Zhu, F. Zhou, W. Zeng, H. Su, G. Li, J. Gao, R. Sun and C. P. Wong, *ACS Nano,* **2016**, *10*, 1273-1282.

31 Tang, M. Chen, C. Yang, W. Wang, H. Bao and G. Wang, *ACS Appl. Mater. Interfaces,* **2015**, *7*, 15303-15313.

32 R. Li, Y. Wang, C. Zhou, C. Wang, X. Ba, Y. Li, X. Huang and J. Liu, *Adv. Funct. Mater.,* **2015**, *25*, 5384-5394.

33 J. Qin, J. Gao, X. Shi, J. Chang, Y. Dong, S. Zheng, X. Wang, L. Feng and Z.-S. Wu, *Adv. Funct. Mater.,* 2020*, 30*, 1909756.

34 S. Liu, J. Xie, H. Li, Y. Wang, H. Y. Yang, T. Zhu, S. Zhang, G. Cao and X. Zhao, *J. Mater. Chem. A,* **2014**, 2, 18125-18131.

35 J. Lin, C. Zhang, Z. Yan, Y. Zhu, Z. Peng, R. H. Hauge, D. Natelson and J. M. Tour, *Nano Lett.,* **2013**, *13*, 72-78.

36 G. Lee, D. Kim, D. Kim, S. Oh, J. Yun, J. Kim, S.-S. Lee and J. S. Ha, *Energy Environ. Sci.,* **2015**, *8*, 1764-1774.

37 L. Li, J. Zhang, Z. Peng, Y. Li, C. Gao, Y. Ji, R. Ye, N. D. Kim, Q. Zhong, Y. Yang, H. Fei, G. Ruan and J. M. Tour, *Adv. Mater.,* **2016**, *28*, 838-845.

38 Y. Yue, Z. Yang, N. Liu, W. Liu, H. Zhang, Y. Ma, C. Yang, J. Su, L. Li, F. Long, Z. Zou and Y. Gao, *ACS Nano,* **2016**, *10*, 11249-11257.

39 J. Y. Hwang, M. F. El-Kady, Y. Wang, L. Wang, Y. Shao, K. Marsh, J. M. Ko and R. B. Kaner, *Nano Energy,* **2015**, *18*, 57-70.

40 Z. Liu, X. Tian, X. Xu, L. He, M. Yan, C. Han, Y. Li, W. Yang and L. Mai, *Nano Res.,* **2017**, *10*, 2471-2481.